SPHERICALLY-ACTUATED PLATFORM MANIPULATOR

Robert L. Williams II
Dana B. Poling
Ohio University
Athens, OH 45701

Final Manuscript
Journal of Robotic Systems

December, 2000

Contact author information:
Robert L. Williams II
Associate Professor
Department of Mechanical Engineering
257 Stocker Center
Ohio University
Athens, OH 45701-2979
phone: (740) 593-1096
fax: (740) 593-0476
email: williar4@ohio.edu
URL: http://www.ent.ohiou.edu/~bobw

SPHERICALLY-ACTUATED PLATFORM MANIPULATOR

Robert L. Williams II and Dana B. Poling
Ohio University
Athens, OH 45701

KEYWORDS: Spherical Actuation, Platform Manipulator, Parallel Robot

ABSTRACT

This article presents the inverse and forward pose and rate kinematics solutions for a novel 6-dof platform manipulator, actuated by two base-mounted spherical actuators. The moving platform is connected to the fixed base by two identical *SPU* serial chain legs. The *S*-joint is active, and the remaining two joints in each chain are passive. An analytical solution is presented for the inverse pose problems, a semi-analytical solution is presented for the rate problems, and the numerical Newton-Raphson technique is employed to solve the forward pose problem. Unfortunately, the passive joint variables cannot be ignored in the kinematics solutions as they can for the Gough/Stewart platform. Examples are presented and hardware has been built, using two Rosheim Omni-Wrists on loan from NASA as the spherical actuators.

1. INTRODUCTION

Parallel robots have been proposed for some time now, due to their potential advantages over serial robots in high load bearing, acceleration, and stiffness, with lower moving mass. A prime disadvantage is reduced workspace relative to serial robots. Hunt[1] did some of the pioneering work in this field. Tsai[2] has recently published a book giving a good overview of the mechanics of parallel robots. There is a rich literature in parallel robots, mostly focusing on forward pose solutions and singularity analysis (e.g. Daniali et al.[3]; Innocenti and Parenti-Castelli[4]; Raghavan[5]; and Wang and Gosselin[6]). Parallel manipulators continue to interest researchers, as seen in the recent literature: work has been presented concerning parallel manipulator dynamics[7], modular platform manipulators[8], and singularity determination in spatial platform manipulators[9].

A major type of parallel robot architecture is the platform manipulator such as the well-known Gough/Stewart platform[10]. This 6-degree-of-freedom (dof) platform is controlled by six prismatic legs, connecting the moving platform in parallel with the base. Interestingly, this platform architecture that has become known as the Stewart platform never appears in ref. [10]. A related architecture is the variable-geometry truss (VGT), such as the double-octahedral design from NASA (Rhodes and Mikulas[11]; inverse pose solutions by Padmanabhan et al.[12]). These two types of parallel robot are designed to be loaded axially only; prismatic (*P*) actuators are generally the control elements, and passive universal (*U*) and spherical (*S*) joints are included to allow the proper freedoms. These types of parallel manipulators have been proposed and used in such applications as flight simulation, machining tools, assembly fixturing, entertainment, space structure modules, and robotic joints for long-reach manipulators.

Many spherical actuation devices have been built or proposed; most of these are developed for use as robotic wrist mechanisms (e.g. the offset "spherical" Omni-Wrist[13] and the truly spherical robot wrists of Roth and Lee[14], and Stanisic and Duta[15]). More recently, various spherical motors have been developed (e.g. Wang et al.[16] and Lee et al.[17]).

The idea that led to the platform manipulator presented in this article is that the (generally passive) spherical joints of a platform manipulator may be instead actively driven; then the remaining *P*, *U*, and other joints are passive. Two active *S* joints are sufficient for a 6-dof platform manipulator. In this article we introduce the Spherically-Actuated platform Manipulator, or SAM. According to a search of the literature, this idea has not been presented before. Potential benefits of this new topology include ground-mounted actuators, new application of recently-available spherical actuators, and compact actuation for 6-dof platforms. A drawback of this proposed manipulator is that not all loads are axial, but the links connected to the active *S*-joints experience moment loading.

Pennock and Mattson[18] study a class of parallel manipulators formed by multiple serial robots grasping a common payload, a one-dof mechanism. In the current work, the inverse pose and rate problems benefit from viewing the platform manipulator as a collection of serial robots with the same control frame (on the moving platform); however it is different from the Pennock work since each serial chain has both active and passive joints, and the platform is rigid.

This idea was first presented in a conference paper[19]. Major improvements were made to that paper: we include analytical solutions for the inverse pose, add rate kinematics, and clear up the singularity issue that was outstanding in the conference paper. The current article focuses on the inverse and forward pose (position and orientation) and rate kinematics solutions for SAM. First, the new platform manipulator architecture is presented, followed by solution of the inverse and forward pose kinematics problems, and then the rate solutions. Trajectory examples are presented to demonstrate the inverse solutions. Finally, a brief discussion covers our hardware design and experimental work.

2. PLATFORM MANIPULATOR DESCRIPTION

The parallel platform manipulator presented in this article (Spherically-Actuated platform Manipulator, SAM) consists of a fixed base and a moving platform connected by two *SPU* (spherical-prismatic-universal joint) serial chain legs (see Figs. 1 and 2). The platform is actuated by two spherical actuators mounted to the base. The passive *U* joints are fixed to the moving platform; the *P* joints are also passive. The mobility is calculated with the Kutzbach equation:

$$\begin{aligned} M &= 6(N-1) - 5J_1 - 4J_2 - 3J_3 \\ M &= 6(6-1) - 5(2) - 4(2) - 3(2) = 6 \end{aligned} \tag{1}$$

This platform manipulator has 6 degrees-of-freedom (dof), provided by the two base-mounted 3-dof spherical actuators. By controlling the six spherical joint variables, general Cartesian poses (positions and orientations) may be reached within a limited workspace. Additional constraining serial *SPU* legs may be used, with all passive joints or another *S* actuator (redundant actuation); the overall mobility will still be six.

In more established platform manipulators such as the Gough/Stewart Platform and variable geometry trusses, the robot is designed such that all loads are axial, avoiding by design the moment loading. This is not the case with our active spherically-driven platform; the links connected to the active *S*-joints experience moment loading. However, other platform manipulators from the literature with *R*-joint actuation suffer from this deficit as well (such as the original Stewart Platform[10]). Another SAM shortcoming is that the inverse pose kinematics is not as straight-forward as it is for the Gough/Stewart platform. Despite these issues, we present the SAM concept to explore spherical actuation of platform manipulators, due to the recent interest in development of spherical actuators. The main focus of this article is SAM kinematics, presented in the next section.

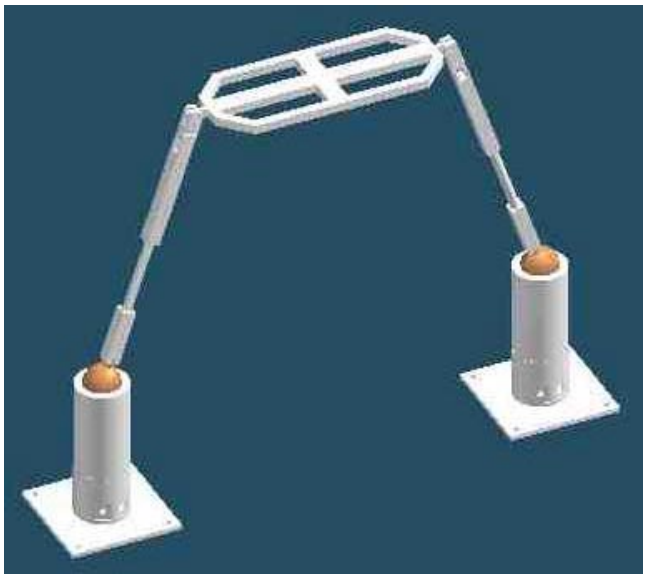

Figure 1. SAM Concept

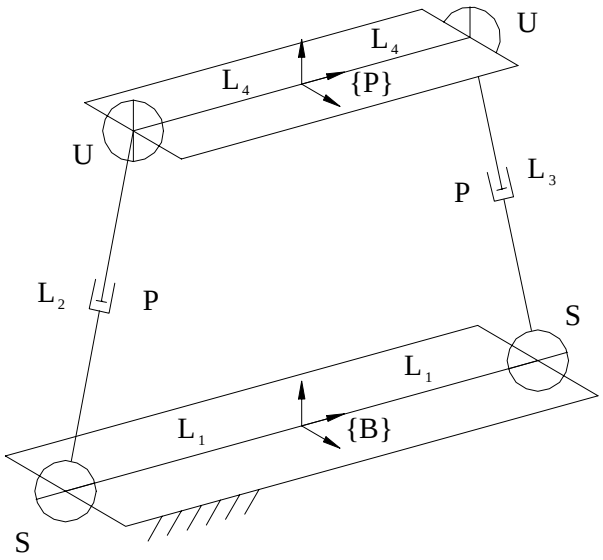

Figure 2. SAM Kinematic Diagram

3. SAM KINEMATICS

This section presents the inverse and forward pose (position and orientation), plus rate kinematics analysis for the SAM robot. Inverse pose (or rate) kinematics is required for platform control; forward pose kinematics is required for platform simulation and sensor-based control. Kinematics is concerned with relating the active joint variables and the platform Cartesian pose variables. Unfortunately, there are also passive, intermediate joint variables which are unknowns in both forward and inverse pose, which complicate these problems. The SAM kinematic diagram is given in Fig. 2.

L_1 is the distance from the base frame $\{B\}$ origin to the fixed location of the left *S*-actuator. L_2 is the total variable passive *P* joint length between the *S* and *U* joints. L_4 is the fixed distance between the moving platform frame $\{P\}$ origin and the *U*-joint location of the left *SPU* leg. The platform manipulator is designed with symmetry for the left and right legs, so lengths L_1 and L_4 also appear on the right *SPU* leg. However, the right *SPU* leg variable passive *P* joint length is L_3.

The detailed kinematic diagram for the left *SPU* serial chain leg is shown in Fig. 3. Figure 3 shows the *X* and *Z* axes for all intermediate coordinate frames, defined according to standard Denavit-Hartenberg parameters for serial robots[20]. The *S*-actuator active joint variables are roll θ_1, yaw θ_2, and

pitch θ_3. The passive joint variables are *P*-joint length L_2 and *U*-joint angles ϕ_2 and ϕ_3. Note the *U*-joint cannot be aligned so that one of its revolute joints is along L_4, in the Y_P direction, or the platform would revolve uncontrollably about this axis (assuming the right *SPU* leg is identical). The Denavit-Hartenberg (DH) parameters for the left *SPU* serial chain leg are given in Table I (angle units are *deg*).

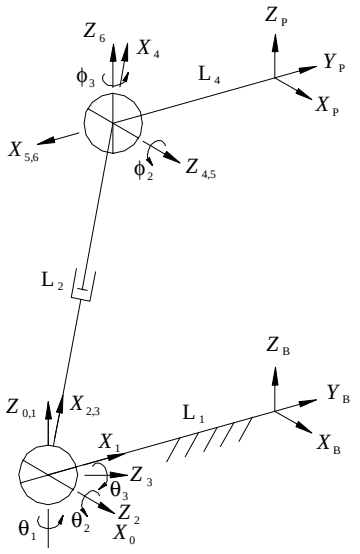

Figure 3. Left SPU *Leg Kinematic Diagram*

Table I. Left *SPU* Leg DH Parameters

i	α_{i-1}	a_{i-1}	d_i	θ_i
1	0	0	0	$\theta_1 + 90$
2	90	0	0	$\theta_2 + 90$
3	90	0	0	θ_3
4	-90	L_2	0	0
5	0	0	0	$\phi_2 + 90$
6	90	0	0	ϕ_3

A word of explanation is in order for the DH parameters chosen for the S-joint in Fig. 3. The model may seem complicated (angle offsets for i=1,2, and L_2 along the X instead of Z axis). This model was adapted from earlier work with the Rosheim Omni-Wrist[21], which is used in our hardware as the spherical actuators. Fixed lengths L_1 and L_4 do not appear in Table I, which relates the *U* joint location to the *S*-actuator base; these two lengths are included via homogeneous transformation matrices later. In our

design the right *SPU* leg is identical to the left. The right *SPU* leg DH parameters are thus identical to Table I, using the following variable substitutions:

$$\begin{aligned} \theta_4 &\rightarrow \theta_1 & \qquad L_3 &\rightarrow L_2 \\ \theta_5 &\rightarrow \theta_2 & \qquad \phi_5 &\rightarrow \phi_2 \\ \theta_6 &\rightarrow \theta_3 & \qquad \phi_6 &\rightarrow \phi_3 \end{aligned}$$

In this section we use a combination of serial chain and parallel chain methods to formulate and solve the SAM pose and rate kinematics problems. The six SAM *S*-actuator joint variables are $\{\theta_1, \theta_2, \theta_3\}$ and $\{\theta_4, \theta_5, \theta_6\}$, respectively. The six Cartesian pose variables are $\{x, y, z, \alpha, \beta, \gamma\}$, related to the homogeneous transformation matrix of the moving platform frame $\{P\}$ with respect to the fixed base frame $\{B\}$:

$$\begin{aligned} {}^B_P T &= \begin{bmatrix} & \left[{}^B_P R\right] & & \left\{{}^B P_P\right\} \\ 0 & 0 & 0 & 1 \end{bmatrix} \\ {}^B_P T &= \begin{bmatrix} c\alpha c\beta & -s\alpha c\gamma + c\alpha s\beta s\gamma & s\alpha s\gamma + c\alpha s\beta c\gamma & x \\ s\alpha c\beta & c\alpha c\gamma + s\alpha s\beta s\gamma & -c\alpha s\gamma + s\alpha s\beta c\gamma & y \\ -s\beta & c\beta s\gamma & c\beta c\gamma & z \\ 0 & 0 & 0 & 1 \end{bmatrix} \end{aligned} \tag{2}$$

Where α, β, γ are *Z-Y-X* Euler angles[20]. The six intermediate variables are left and right *SPU* leg passive variables $\{L_2, \phi_{2,}\phi_3\}$ and $\{L_3, \phi_{5,}\phi_6\}$, respectively.

Now we formulate and solve the SAM inverse and forward pose kinematics problems using the kinematic diagrams, Denavit-Hartenberg parameters, and variables described. This is followed by rate kinematics.

3.1 Inverse Pose Kinematics

The SAM inverse pose kinematics problem is stated: Given the desired Cartesian platform pose $\{x, y, z, \alpha, \beta, \gamma\}$ (or, equivalently, ${}^{B}_{P}T$), calculate the required *S*-actuator joint variables $\{\theta_1, \theta_2, \theta_3\}$ and $\{\theta_4, \theta_5, \theta_6\}$. The left- and right-leg passive joint variables $\{L_2, \phi_{2,} \phi_3\}$ and $\{L_3, \phi_{5,} \phi_6\}$ are also unknowns. The passive variables are not required for real-time control, but they may be used in on-line rate and dynamics equations, plus off-line for simulation.

This inverse pose problem is solved by considering the left and right *SPU* serial chain legs separately. The given Cartesian pose ${}^{B}_{P}T$ must be reached by both legs, each with three active and three passive joints. Thus, the problem decouples between the left and right legs. Below we describe the procedure for the left *SPU* leg; the right is the same, with the above-noted variable substitutions.

To solve the left-leg active and passive joint variables given the Cartesian pose ${}^{B}_{P}T$, we first extract numbers for ${}^{0}_{6}T$ from the given ${}^{B}_{P}T$:

$$ {}^{0}_{6}T = {}^{B}_{0}T^{-1} \, {}^{B}_{P}T \, {}^{6}_{P}T^{-1} \tag{3} $$

where, from Fig. 3:

$$ {}^{B}_{0}T = \begin{bmatrix} 1 & 0 & 0 & 0 \\ 0 & 1 & 0 & -L_1 \\ 0 & 0 & 1 & 0 \\ 0 & 0 & 0 & 1 \end{bmatrix} \qquad {}^{6}_{P}T = \begin{bmatrix} 0 & -1 & 0 & -L_4 \\ 1 & 0 & 0 & 0 \\ 0 & 0 & 1 & 0 \\ 0 & 0 & 0 & 1 \end{bmatrix} $$

Equation (3) brings fixed parameters L_1 and L_4 into the process. Now, this inverse pose problem may be solved more easily by inverting our view: consider the *S*-actuator to be the wrist of a serial chain which is translated by joints $\{L_2, \phi_{2,} \phi_3\}$. Since the "wrist" is spherical we may first solve for $\{L_2, \phi_{2,} \phi_3\}$ from the translational terms of the (numerically) inverted ${}^{6}_{0}T = {}^{0}_{6}T^{-1}$. Extract the fourth column of ${}^{6}_{0}T$ and define $\{{}^{6}P_0\} = \{X_1 \quad Y_1 \quad Z_1\}^T$ (known numbers from the given command). The equations to solve are:

$$\begin{aligned} X_1 &= L_2 s\phi_2 c\phi_3 \\ Y_1 &= -L_2 s\phi_2 s\phi_3 \\ Z_1 &= -L_2 c\phi_2 \end{aligned} \tag{4}$$

where $c\phi_2 = \cos(\phi_2), s\phi_2 = \sin(\phi_2)$, and so on. The solutions are:

$$\begin{aligned} L_2 &= +\sqrt{X_1^2 + Y_1^2 + Z_1^2} \\ \phi_3 &= \text{atan2}(-Y_1, X_1) \\ \phi_2 &= \text{atan2}(X_1 / c\phi_3, -Z_1) \end{aligned} \tag{5}$$

Only the positive square root is used for L_2 due to physical *P*-joint constraints. In the rare case that $\phi_3 = 90^\circ$, the solution for ϕ_2 suffers from an algorithmic singularity and the alternate solution $\phi_2 = \text{atan2}(-Y_1 / s\phi_3, -Z_1)$ may be used instead. There are two solution sets, a single L_2, with (ϕ_3, ϕ_2) and $(\phi_3 + \pi, -\phi_2)$.

Now that $\{L_2, \phi_2, \phi_3\}$ are known, we can solve for $\{\theta_1, \theta_2, \theta_3\}$; we needn't use the inverted view in this case. First, extract numbers for ${}^0_3R$ from the known ${}^0_6R$ and the newly-calculated ${}^3_6R$:

$${}^0_3R = {}^0_6R\,{}^3_6R^T \tag{6}$$

where:

$${}^3_6R = \begin{bmatrix} -s\phi_2 c\phi_3 & s\phi_2 s\phi_3 & c\phi_2 \\ s\phi_3 & c\phi_3 & 0 \\ -c\phi_2 c\phi_3 & c\phi_2 s\phi_3 & -s\phi_2 \end{bmatrix}$$

Equate the numbers for ${}^0_3R$ with the symbolic formulas:

$${}^0_3R = \begin{bmatrix} r_{11} & r_{12} & r_{13} \\ r_{21} & r_{22} & r_{23} \\ r_{31} & r_{32} & r_{33} \end{bmatrix} = \begin{bmatrix} K_1 & K_3 & -s_1 c_2 \\ K_2 & K_4 & c_1 c_2 \\ c_2 c_3 & -c_2 s_3 & s_2 \end{bmatrix} \tag{7}$$

where:

$$\begin{aligned} K_1 &= c_1 s_3 + s_1 s_2 c_3 & \qquad K_3 &= c_1 c_3 - s_1 s_2 s_3 \\ K_2 &= s_1 s_3 - c_1 s_2 c_3 & \qquad K_4 &= s_1 c_3 + c_1 s_2 s_3 \end{aligned}$$

and $c_1 = \cos(\theta_1), s_1 = \sin(\theta_1)$, and so on. From (7), the solutions are:

$$\begin{aligned}\theta_1 &= \text{atan2}(-r_{13}, r_{23}) \\ \theta_2 &= \text{atan2}(r_{33}, r_{23}/c_1) \\ \theta_3 &= \text{atan2}(-r_{32}, r_{31})\end{aligned} \tag{8}$$

For completeness, the *signs* of c_2 should be taken into account in the atan2 functions; however since both θ_1 and θ_3 have multiple solutions (the above, also the above plus π radians), this trigonometric uncertainty does not matter. There is one θ_2 solution for each θ_1. To avoid the algorithmic singularity when $\theta_1 = 90^\circ$, use the alternate solution $\theta_2 = \text{atan2}(r_{33}, -r_{13}/s_1)$.

There are four solution sets to the overall left *SPU* leg inverse pose problem (the first row below comes from (8) and (5)):

Table II. Multiple Inverse Pose Solutions, Left *SPU* Leg

θ_1	θ_2	θ_3	L_2	ϕ_2	ϕ_3
$\theta_1 + \pi$	$\pi - \theta_2$	$\theta_3 + \pi$	L_2	ϕ_2	ϕ_3
$\theta_1 + \pi$	$-\theta_2$	$-\theta_3$	L_2	$-\phi_2$	$\phi_3 + \pi$
θ_1	$\pi + \theta_2$	$\pi - \theta_3$	L_2	$-\phi_2$	$\phi_3 + \pi$

Generally only the first row in Table II applies to our SAM design.

In this manner, the inverse pose kinematics problem for the left *SPU* portion of SAM is solved. The right-leg portion is solved following this, independently in exactly the same manner, using the above-mentioned variable substitutions; the unknowns are $\{\theta_4 \quad \theta_5 \quad \theta_6 \quad L_3 \quad \phi_5 \quad \phi_6\}^T$. We also need to reverse the signs of L_1 and L_4 (see Figs. 2 and 3) in the fixed transformation matrices from (3).

3.2 Forward Pose Kinematics

The SAM forward pose kinematics problem is stated: Given the *S*-actuator joint variables $\{\theta_1 \quad \theta_2 \quad \theta_3 \quad \theta_4 \quad \theta_5 \quad \theta_6\}^T$, calculate the associated Cartesian platform pose $\{x, y, z, \alpha, \beta, \gamma\}$ (or, equivalently, ${}^B_P T$ as in (2)). The left- and right-leg passive joint variables $\{L_2, \phi_{2,} \phi_3\}$ and $\{L_3, \phi_{5,} \phi_6\}$ are again unknowns as well.

This forward pose problem cannot be solved by considering the left and right *SPU* serial chain legs separately. The problem is coupled because both *SPU* serial chain legs share the same Cartesian unknowns. Standard serial robot kinematics techniques cannot be used in the SAM forward pose solution since the intermediate passive joint variables are unknown. We tried to develop an analytical solution but found that the equations do not decouple like the analytical inverse pose solution of the previous section. We will solve this problem numerically from the basic equations via Newton-Raphson iteration. The details for this are presented in Williams and Poling[19] and will not be repeated here.

However, a simplified approach is described here. In that conference paper, we solved the forward pose problem for the full twelve equations in the twelve unknowns. The approach we have now implemented ignores unknowns $\{x, y, z, \alpha, \beta, \gamma\}$ at first; thus the system size is cut in half. Using the DH parameters for the left and right legs, plus the fixed transformation matrices from (3) (again, reversing the signs of L_1 and L_4 for the right leg), the symbolic form for ${}^{B}_{P}T$ is derived twice (for the left and right legs, ${}^{B}_{P}T_{LEFT}$ and ${}^{B}_{P}T_{RIGHT}$, respectively) using standard serial chain robotics techniques[20]. ${}^{B}_{P}T_{LEFT}$ is a function of knowns $\{\theta_1, \theta_2, \theta_3\}$ and unknowns $\{L_2, \phi_2, \phi_3\}$; ${}^{B}_{P}T_{RIGHT}$ is a function of knowns $\{\theta_4, \theta_5, \theta_6\}$ and unknowns $\{L_3, \phi_5, \phi_6\}$.

To produce the functions for Newton-Raphson to solve, we simply equate the symbolic forms, ${}^{B}_{P}T_{LEFT} = {}^{B}_{P}T_{RIGHT}$. The three translational terms provide independent equations and three of the nine rotational terms provide the remaining three required equations. All three rotational equations cannot come from one row or column due to the fact that an orthonormal rotation matrix row or column is constrained to be a unit vector. Algorithmic singularities were encountered in the nominal horizontal SAM configuration when using certain rotational equations; we used the (2,1), (2,2), and (3,2) terms to overcome this problem. An attempt was made to solve these equations analytically; this did not succeed since the three translational equations are coupled in the six unknowns, while the three rotational

equations are coupled in four unknowns (all except L_2 and L_3). Using Newton-Raphson iteration (as in Williams and Poling[19], but with this reduced set of equations) we solve for $\{L_2 \quad \phi_2 \quad \phi_3 \quad L_3 \quad \phi_5 \quad \phi_6\}^T$ given $\{\theta_1 \quad \theta_2 \quad \theta_3 \quad \theta_4 \quad \theta_5 \quad \theta_6\}^T$. Following this, it is a simple matter to calculate the Cartesian unknowns $\{x, y, z, \alpha, \beta, \gamma\}$ from ${}^B_P T_{LEFT}$ evaluated with $\{\theta_1, \theta_2, \theta_3\}$ and $\{L_2, \phi_2, \phi_3\}$, or ${}^B_P T_{RIGHT}$ evaluated with $\{\theta_4, \theta_5, \theta_6\}$ and $\{L_3, \phi_5, \phi_6\}$.

The Newton-Raphson approach to solving forward pose kinematics suffers from the need of a good initial guess, and only one of the multiple solutions is found. However, in practical real-time control these do not present problems since we know the value of all variables at the previous control cycle, including a starting configuration. Also, the single solution found will be the one closest to the initial guess; assuming a fast control rate, the proper solution will generally be found.

3.3 Rate Kinematics

Rate kinematics is concerned with relating the active joint rates and the platform Cartesian rates; again, intermediate joint rates are involved as well. All pose variables must be known first. The inverse velocity solution, which is the basis of the resolved-rate control scheme, is stated: given the commanded platform Cartesian rates $\dot{X} = \{\dot{x} \quad \dot{y} \quad \dot{z} \quad \omega_x \quad \omega_y \quad \omega_z\}^T$, calculate the associated active joint rates $\dot{\Theta} = \{\dot{\theta}_1 \quad \dot{\theta}_2 \quad \dot{\theta}_3 \quad \dot{\theta}_4 \quad \dot{\theta}_5 \quad \dot{\theta}_6\}^T$. The Cartesian rate $\dot{X}$ gives the translational and rotational rates of $\{P\}$ with respect to $\{B\}$, expressed in a certain frame ($\{B\}$ in our work). As in the inverse pose solution, the inverse rate solution decouples between the left and right legs. Using standard serial robotics methods, two Jacobian matrices are used:

$$\dot{X} = J_L \dot{\Theta}_L \qquad\qquad \dot{X} = J_R \dot{\Theta}_R \tag{9}$$

where: $\dot{\Theta}_L = \{\dot{\theta}_1 \quad \dot{\theta}_2 \quad \dot{\theta}_3 \quad \dot{L}_2 \quad \dot{\phi}_2 \quad \dot{\phi}_3\}^T$ $\qquad$ $\dot{\Theta}_R = \{\dot{\theta}_4 \quad \dot{\theta}_5 \quad \dot{\theta}_6 \quad \dot{L}_3 \quad \dot{\phi}_5 \quad \dot{\phi}_6\}^T$

$\dot{X}$, defined above, is the common platform Cartesian velocity that must be achieved simultaneously by both serial *SPU* chains. J_L is the left-leg Jacobian matrix mapping the left leg joint rates (active and passive) to the Cartesian rates and J_R is the right-leg Jacobian matrix mapping the right leg joint rates (active and passive) to the same Cartesian rates. The decoupled inverse rate solutions are:

$$\dot{\Theta}_L = J_L^{-1}\dot{X} \qquad\qquad \dot{\Theta}_R = J_R^{-1}\dot{X} \tag{10}$$

Equations (10) are sufficient for use in real-time resolved-rate control. This is a semi-analytical solution since the Jacobian matrices are available symbolically, but we invert these numerically for (10).

Using a fully-symbolic approach, one could solve the inverse rate problem in one step, ignoring the passive joint rates. This approach inverts the Jacobian matrices symbolically off-line. Equations (10) map the common Cartesian velocity to joint rates; therefore we select just the first three rows of each symbolic inverse Jacobian matrix, which maps the Cartesian velocity only to active joint rates. Denote the top three rows of the symbolic inverse Jacobian matrices as J_{LA}^{-1} and J_{RA}^{-1}, respectively (*A* indicates active joints only). The one-step inverse rate solution is then:

$$\dot{\Theta} = M\dot{X} \tag{11}$$

where: $M = \begin{bmatrix} J_{LA}^{-1} \\ J_{RA}^{-1} \end{bmatrix}$ and $\dot{\Theta} = \begin{Bmatrix} \dot{\theta}_1 & \dot{\theta}_2 & \dot{\theta}_3 & \dot{\theta}_4 & \dot{\theta}_5 & \dot{\theta}_6 \end{Bmatrix}^T$.

With this approach, the overall forward velocity solution is:

$$\dot{X} = M^{-1}\dot{\Theta} \tag{12}$$

Even though the symbolic Jacobian matrices for the left and right legs of SAM are relatively simple (few terms), this approach yields very complex results when using a symbolic computer program. Therefore, we use the partial-analytical method described above, with (10).

One benefit of rate analysis is that singularity analysis follows from setting the Jacobian matrix determinants to zero:

$$\left|J_L\right| = L_2^2 c_2 s\phi_2 = 0 \qquad \left|J_R\right| = L_3^2 c_5 s\phi_5 = 0 \tag{13}$$

From these singularity equations, the SAM singular conditions are:

$$\begin{array}{lll} L_2 = 0 & \theta_2 = \pm 90^\circ & \phi_2 = 0,180^\circ \\ L_3 = 0 & \theta_5 = \pm 90^\circ & \phi_5 = 0,180^\circ \end{array} \tag{14}$$

The left-most conditions in (14) can never occur. The middle conditions are on the extreme workspace boundary for the *S*-actuators in our hardware design. The right-most singular conditions (0, not 180°) are the only ones that exist for SAM. These correspond to when the left ($\phi_2 = 0$) or right ($\phi_5 = 0$) *SPU* leg is normal to the platform. In this case, the Jacobian row corresponding to ω_y is not independent; there is no way to rotate about the Y_p axis in this configuration. The Jacobian determinants should be monitored on-line; when one approaches zero, the pseudoinverse of the offending Jacobian matrix should be used in (10). The motion will not be exactly as commanded, but this will provide a numerically-stable means to move the robot through the singular condition.

4. EXAMPLES

This section presents a snapshot example, followed by trajectory examples to demonstrate results from the inverse pose and rate kinematics solutions presented in Section 3.

4.1 A Nominal Configuration

A good nominal configuration for this platform manipulator is a pose like that shown in Fig. 1: the platform is level, $\{P\}$ is translated relative to $\{B\}$ only in the vertical Z direction, and the orientations of $\{P\}$ and $\{B\}$ are aligned. The SAM design parameters are: L_1 = 0.5334 and L_4 = 0.3556 (m). Choosing a nominal angle of $\theta_2 = -15^\circ$, the active joint parameters, Cartesian pose, and passive joint variables, respectively, for this configuration are given below and shown in Fig. 4. Length units are *m* and angular units are *deg*.

$$\begin{aligned} \{\theta_1 \quad \theta_2 \quad \theta_3 \quad \theta_4 \quad \theta_5 \quad \theta_6\} &= \{0 \quad -15 \quad 0 \quad 0 \quad 15 \quad 0\} \\ \{x \quad y \quad z \quad \alpha \quad \beta \quad \gamma\} &= \{0 \quad 0 \quad 0.664 \quad 0 \quad 0 \quad 0\} \\ \{L_2 \quad \phi_2 \quad \phi_3 \quad L_3 \quad \phi_5 \quad \phi_6\} &= \{0.687 \quad 15 \quad 0 \quad 0.687 \quad -15 \quad 0\} \end{aligned} \tag{15}$$

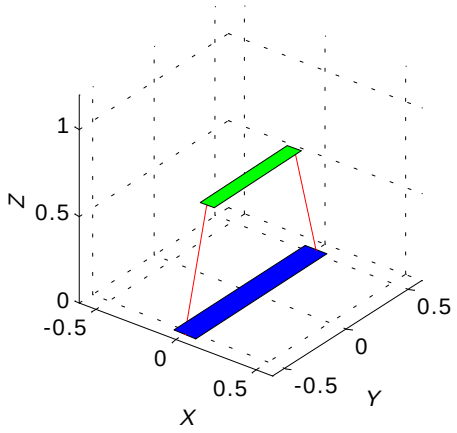

Figure 4. Nominal SAM Configuration for Examples

4.2 Trajectories with Inverse and Forward Pose Solutions

Starting from this nominal pose, we now present trajectory examples for the inverse pose and rate solutions. To demonstrate the *inverse pose solutions*, we start at the Cartesian pose from the middle line of (15). At each step, we add $\{0.005, 0.005, 0.005, 0, 0, 0.5^\circ\}$ to the specified Cartesian pose. That is, we

are translating by 5 *mm* in all *X*,*Y*,*Z* axes, and rotating $\gamma = 0.5^\circ$ about the *X* axis in each of ten simulated time steps. Figures 5a and 5b present the left and right actuator inverse pose solution results. In Fig. 5a, θ_1 is solid, θ_2 dashed, and θ_3 dot-solid; in Fig. 5b, θ_4 is solid, θ_5 dashed, and θ_6 dot-solid.

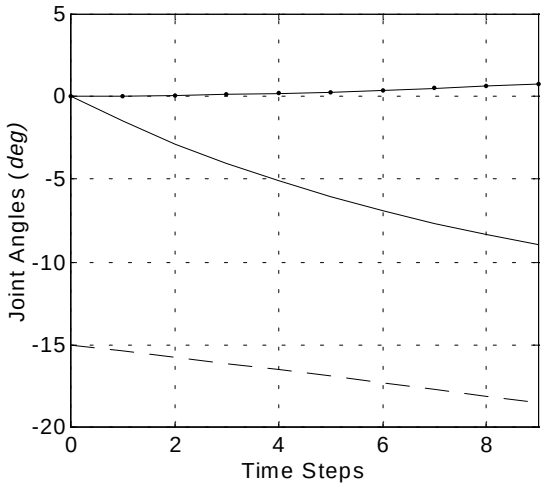

Figure 5a. Inverse Pose Results, Left S*-Actuator*

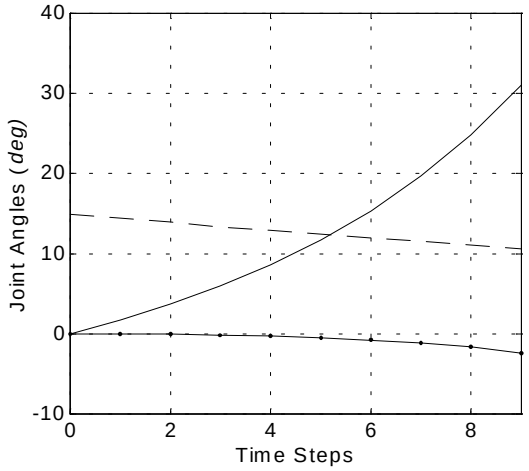

Figure 5b. Inverse Pose Results, Right S*-Actuator*

Figures 5 show the joint angles required to achieve the commanded Cartesian motion (equal positive steps of 5 *mm* in the *X*, *Y*, and *Z* directions, while simultaneously twisting the platform 0.5° about the *Z* axis in each simulated time step). The spherical actuator joint angles each start at the nominal configuration given in the top line of (15) and change smoothly throughout the motion. The largest angle changes are experienced by joints 1 and 4 (starting at 0 and moving in opposite directions), which makes sense for the twisting of the platform. Joints 3 and 6 require the least motion (again starting at 0 and moving in opposite directions). Joints 2 and 5, responsible for pitching the SPU legs, start at their respective initial angles and move in the same direction.

Assuming a nominal control rate of 100 Hz (achievable in the laboratory hardware of Section 5), the simulated Cartesian motions are very large. In practice, the Cartesian trajectory steps would be smaller. This serves to challenge our numerical forward kinematics algorithms and the results are smooth.

To demonstrate the *inverse rate solutions*, we again start at the nominal pose of (15). The commanded Cartesian rate is $\dot{X} = \{-0.1,-0.1,0.1,0.1,0.1,0.1\}^T$ (*m*/*s* and *rad*/*s*). Figures 6a and 6b present the left and right actuator inverse rate solution results, respectively. The joint rates reported in Figs. 6 would be integrated to commanded angles to implement the resolved-rate control in practice. In Fig. 6a, $\dot{\theta}_1$ is solid, $\dot{\theta}_2$ dashed, and $\dot{\theta}_3$ dot-solid; in Fig. 6b, $\dot{\theta}_4$ is solid, $\dot{\theta}_5$ dashed, and $\dot{\theta}_6$ dot-solid.

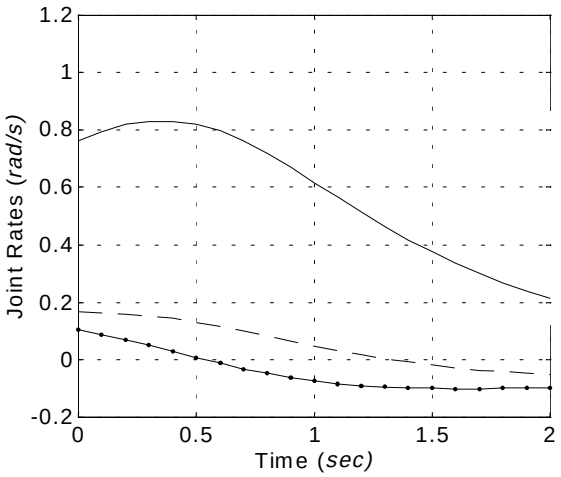

Figure 6a. Inverse Rate Results, Left Actuator

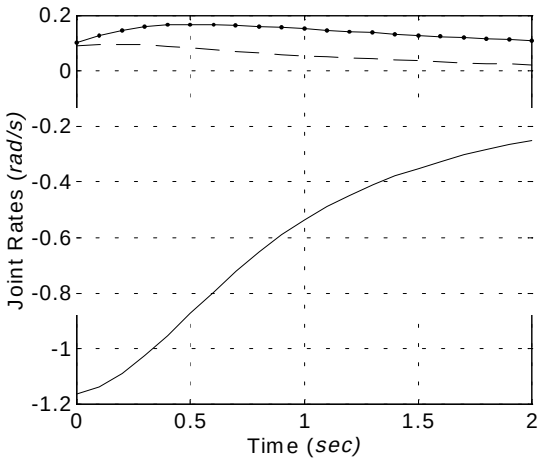

Figure 6b. Inverse Rate Results, Right Actuator

Figures 6 show the joint rates required to achieve the commanded Cartesian rates (equal rates in the -*X*, -*Y*, and +*Z* directions, while simultaneously rotating with equal angular velocity components about the moving +*X*, +*Y*, and +*Z* axes). The initial spherical actuator joint rates are all non-zero since the simulation turns on the Cartesian rate at the start. The joint rates all change smoothly throughout the motion. The commanded trajectory is different from the inverse pose example above. Again, the highest joint motions correspond to joints 1 and 4 (moving in opposite directions). The remaining joints rates are smaller. Joints 2 and 3 each switch directions, while joints 5 and 6 remain positive for the simulated resolved-rate motion.

5. HARDWARE

Figure 7 is a photograph of the spherically-actuated platform manipulator (SAM) hardware designed and built at Ohio University, where the spherical actuators are two Omni-Wrists[13] on loan from NASA Langley Research Center. There are two major differences from the design presented thus far: 1) The spherical actuators are not truly spherical but have a complicating offset; and 2) The two serial chain legs use passive revolute (*R*) joints in place of the passive *P* joints. Difference 1) complicates the kinematics equations so that only numerical solutions are used[19]. Difference 2) was employed originally to make the construction easier. However, we have since discovered that this design has an unwanted singularity for all horizontal orientations ($\alpha = \beta = 0$), in the vertical plane containing the two spherical actuators: in these special configurations, the *RUUR* closed chain acts as a four-bar linkage with an additional, unwanted and uncontrollable degree of freedom. Therefore, we are currently modifying the hardware to use *SPU* legs as in Fig. 1; no such singularity exists for this case. An additional improvement would be to substitute zero-offset spherical actuators for the Omni-Wrists. A third improvement we are considering is to make the moving platform an equilateral triangle and to add a third constraining *SPU* leg (whose *S* joint is passive; alternatively we could add a third spherical actuator which would result in overactutation, which may have stiffness benefits). This would reduce the workspace but improve the force capabilities of the platform.

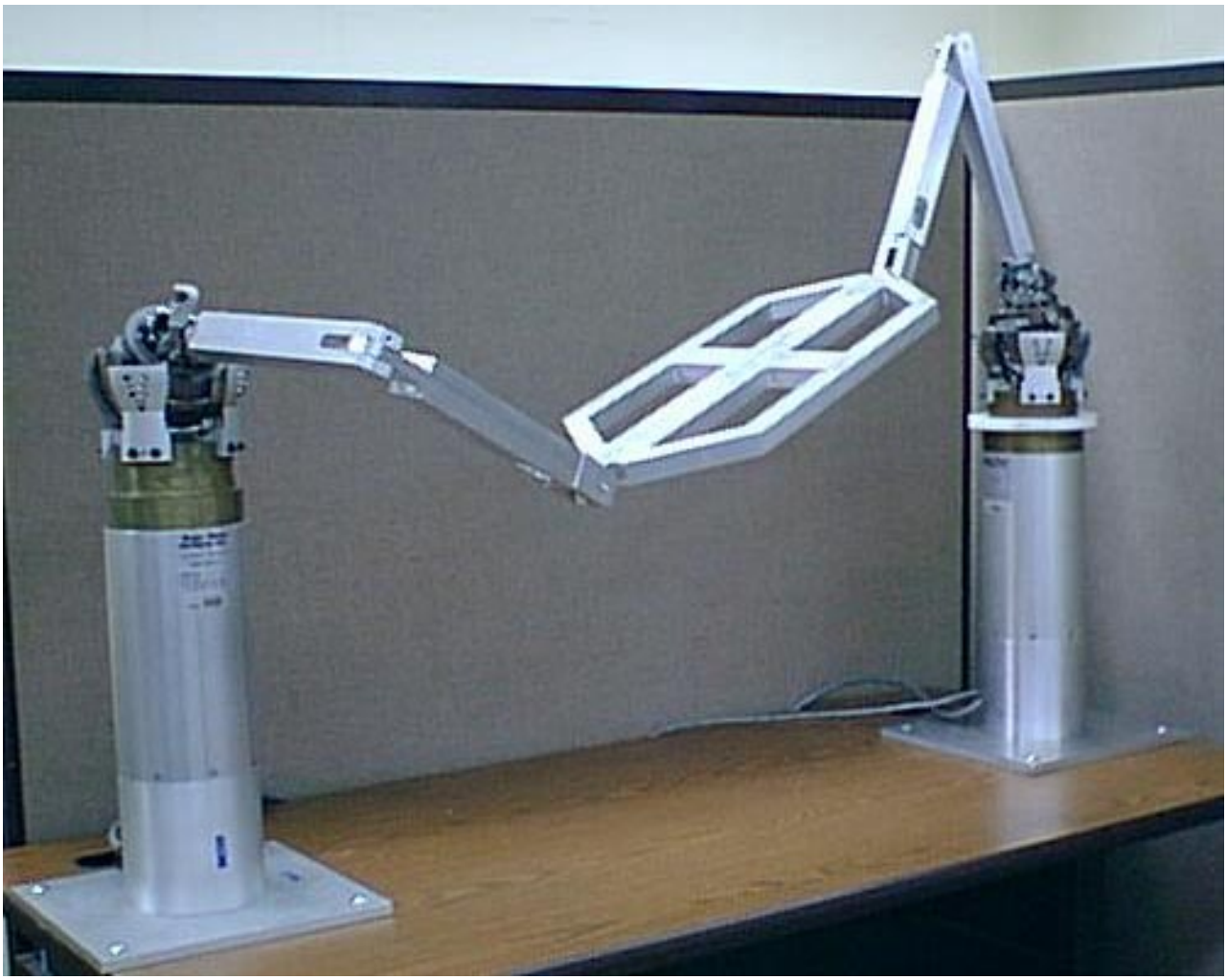

Figure 7. SAM Hardware with SRU Chains and Omni-Wrist Actuators

6. CONCLUSION

This article presents the inverse and forward pose and rate kinematics of a novel platform manipulator, the Spherically-Actuated platform Manipulator, or SAM. This manipulator has a drawback compared with prismatically-actuated platforms: there is moment loading at the actuators (not all loads are axial). Platform manipulators with *R*-joint actuation proposed in the literature also have this disadvantage. However, there has been significant interest in development of spherical actuators recently, which motivates this work. Also, potential benefits include compact, ground mounted actuation for 6-dof platforms.

SAM consists of two *SPU* serial chain legs (*S* active, *P*-*U* passive) connecting the moving platform to the fixed base. The inverse pose problem is solved analytically, the forward pose problems via the numerical Newton-Raphson method, and the inverse rate kinematics problem is solved semi-analytically (symbolic serial-chain Jacobian matrices, numerical inversion). Examples were presented to demonstrate results from the inverse pose and rate kinematics solution algorithms. SAM hardware has been built (*SRU* legs instead of *SPU* legs); we are currently converting this hardware to the *SPU* legs to avoid the uncontrolled four-bar singularity that occurs in nominal orientations of the *SRU* version. The *SPU* SAM singularities have been enumerated and do not pose a serious problem.

REFERENCES

1. K.H. Hunt, 1983, "Structural Kinematics of In-Parallel-Actuated Robot Arms", Journal of Mechanisms, Transmissions, and Automation in Design, 105(4): 705-712.
2. L.-W. Tsai, 1999, **Robot Analysis: The Mechanics of Serial and Parallel Manipulators**, John Wiley & Sons, Inc., New York.
3. H.R.M. Daniali, P.J. Zsombor-Murray, and J. Angeles, 1995, "The Kinematics of Spatial Double-Triangular Parallel Manipulators", Journal of Mechanical Design, 117(4): 658-661.
4. C. Innocenti and V. Parenti-Castelli, 1993, "Forward Kinematics of The General 6-6 Fully Parallel Mechanism: An Exhaustive Numerical Approach Via a Mono-Dimensional-Search Algorithm", Journal of Mechanical Design, 115(4): 932-937.
5. M. Raghavan, 1993, "The Stewart Platform of General Geometry has 40 Configurations", Journal of Mechanical Design, 115(2): 277-280.
6. J. Wang and C.M. Gosselin, 1997, "Kinematic Analysis and Singularity Representation of Spatial Five-degree-of-freedom Parallel Mechanisms", Journal of Robotic Systems 14(12): 851-869.
7. N.D. Perreira, "Motions, Efforts, and Actuations in Constrained Dynamic Systems: A Multilink Closed Chain Example", Journal of Robotic Systems 16 (1999), 363-385.
8. J. Zhiming and L. Zhenqun, "Identification of Placement Parameters for Modular Platform Manipulators", Journal of Robotic Systems 16 (1999), 227-236.
9. F. Hao, J.M. McCarthy, "Conditions for Line-Based Singularities in Spatial Platform Manipulators", Journal of Robotic Systems 15 (1998), 43-55.
10. D. Stewart, 1966, "A Platform with Six Degrees of Freedom", Proceedings of the Institute of Mechanical Engineers (London), 180(15): 371-386.
11. M.D. Rhodes and M.M. Mikulas, 1985, "Deployable Controllable Geometry Truss Beam", NASA Technical Memorandum 86366.
12. B. Padmanabhan, V. Arun, and C.F. Reinholtz, 1992, "Closed-Form Inverse Kinematic Analysis of Variable-Geometry Truss Manipulators", Journal of Mechanical Design, 114(3): 438-443.
13. M.E. Rosheim, 1987, “Singularity-Free Hollow Spray Painting Wrists”, Robots 11 Conference Proceedings RI/SME, Chicago, IL, 13.7-13.28.
14. R.B. Roth and K.-M. Lee, 1995, “Design Optimization of a Three Degrees-of-Freedom Variable-Reluctance Spherical Wrist Motor”, Journal of Engineering for Industry, 117(3): 378-388.
15. M.M. Stanisic and O. Duta, 1990, "Symmetrically Actuated Double Pointing Systems: The Basis of Singularity-Free Robot Wrists", IEEE Transactions on Robotics and Automation, 6(5): 562-569.
16. J. Wang, W. Wang, G.W. Jewell, D. Howe, 1998, “Novel Spherical Permanent Magnet Actuator with Three Degrees-of-Freedom”, IEEE Transactions on Magnetics, 34(4): 2078-2080.
17. K.M. Lee, R.B. Roth, and Z. Zhou, 1996, "Dynamic Modeling and Control of a Ball-joint-Like Variable Reluctance Spherical Motor", Jnl of Dynamic Syst, Measurement, and Control, 118(1): 29-40.
18. G.R. Pennock and K.G. Mattson, 1995, "Forward Position Analysis of Two 3-R Robots Manipulating a Planar Linkage Payload", Journal of Mechanical Design, 117(2): 292-297.
19. R.L. Williams II and D.B. Poling, 2000, "Spherically-Actuated Platform Manipulator", DETC2000/MECH-14111, 26th ASME Mechanisms Conference, Baltimore, MD.
20. J.J. Craig, 1989, **Introduction to Robotics: Mechanics and Control**, Addison Wesley Publishing Co., Reading, MA.
21. R.L. Williams II, 1999, "Inverse Kinematics and Singularities of Manipulators with Offset Wrist", IASTED International Journal of Robotics and Automation, 14(1): 1-8.